

Problems with interpretation of ^{10}He ground state

L. V. Grigorenko^{1,2,3} and M. V. Zhukov⁴

¹*Flerov Laboratory of Nuclear Reactions, JINR, RU-141980 Dubna, Russia*

²*Gesellschaft für Schwerionenforschung mbH, Planckstrasse 1, D-64291, Darmstadt, Germany*

³*RRC “The Kurchatov Institute”, Kurchatov sq. 1, 123182 Moscow, Russia*

⁴*Fundamental Physics, Chalmers University of Technology, S-41296 Göteborg, Sweden*

(Dated: September 26, 2018. File: /latex/10he/10he-17.tex)

The continuum of ^{10}He nucleus is studied theoretically in a three-body $^8\text{He}+n+n$ model basing on the recent information concerning ^9He spectrum [Golovkov, *et al.*, Phys. Rev. C **76**, 021605(R) (2007)]. The ^{10}He ground state (g.s.) candidate with structure $[p_{1/2}]^2$ for new g.s. energy of ^9He is predicted to be at about 2.0–2.3 MeV. The peak in the cross section associated with this state may be shifted to a lower energy (e.g. ~ 1.2 MeV) when ^{10}He is populated in reactions with ^{11}Li due to peculiar reaction mechanism. Formation of the low-energy ($E < 250$ keV) “alternative” ground state with structure $[s_{1/2}]^2$ is highly probable in ^{10}He in the case of considerable attraction (e.g. $a < -5$ fm) in the s -wave ^9He channel, which properties are still quite uncertain. This result either questions the existing experimental low-energy spectrum of ^{10}He or place a limit on the scattering length in ^9He channel, which contradicts existing data.

PACS numbers: 21.60.Gx, 21.45.+v, 25.10.+s, 21.10.Dr

I. INTRODUCTION

The first, at that moment theoretical, attempt to study ^{10}He was undertaken in the end of 60-th [1]. In this work a possibility of the nuclear-stable ^{10}He existence was investigated in the microscopic 10-body hyperspherical harmonic (HH) model. However, until now the ^{10}He nucleus remains relatively poorly studied system. Since it became clear that ^{10}He is nuclear unstable [2] and ground state properties of ^9He were defined [3, 4], it became possible to predict theoretically the ground state of ^{10}He as a narrow three-body $^8\text{He}+n+n$ resonance. It was found with $E \sim 0.7 - 0.9$, $\Gamma \sim 0.1 - 0.3$ MeV [5], for valence neutrons populating mainly $[p_{1/2}]^2$ configuration (the energy E in the present work is always given relative to the three-body $^8\text{He}+n+n$ threshold). These predictions were soon confirmed experimentally: $E = 1.2(3)$, $\Gamma < 1.2$ MeV [6], $E = 1.07(7)$, $\Gamma = 0.3(2)$ MeV [7, 8], and $E = 1.7 \pm 0.3 \pm 0.3$ MeV [9].

A new possible theoretical understanding of ^{10}He was proposed after the existence of a virtual state in ^9He was demonstrated by Chen *et al.* in Ref. [10]. An *upper* limit for scattering length $a < -10$ fm was established in this experimental work. For such an attractive s -wave interaction in ^9He Aoyama predicted in Ref. [11] the existence of a narrow near-threshold 0^+ state in ^{10}He ($E = 0.05$, $\Gamma = 0.21$ MeV) with the $[s_{1/2}]^2$ structure in addition to the $[p_{1/2}]^2$ state (calculated in this work to be at about 1.7 MeV). Concerning evident discrepancy with the experimental data the author of Ref. [11] suggested that the ground state (g.s.) of ^{10}He had not been observed so far and the state at ~ 1.3 MeV is actually the first excited state. However, no possible explanation was proposed in Ref. [11] for which reason the $[s_{1/2}]^2$ g.s. was missed in experiments.

In recent experiment by Golovkov *et al.* [12] at Dubna radioactive beam facility ACCULINNA the low-lying

spectrum of ^9He was revised, providing a higher position of the $p_{1/2}$ state than in the previous studies. A broad $p_{1/2}$ state was observed at about 2 MeV instead of the (presumably) $p_{1/2}$ - $p_{3/2}$ doublet of narrow states at 1.27 and 2.4 MeV as in Refs. [3, 4, 8]. The experiment [12] also claims a unique spin-parity identification below 5 MeV. The presence of the $s_{1/2}$ contribution is evident in the data [12], but the exact nature of this contribution is still unclear, whether it is a virtual state with considerably large negative scattering length or just a smooth nonresonant background. A relaxed *lower* limit for scattering length $a > -20$ fm was established in this work. These new data should have a strong impact on the calculated properties of ^{10}He , which inspired us to “revisit” the issue.

We study the question in theoretical models, which are schematic but have a clear relevance to real possible reaction mechanisms of the ^{10}He continuum population. In a contrast with approach of Ref. [11], which provided only energies and widths of the states, we are interested in the observable consequences of the $J^\pi = 0^+$ states with structures $[s_{1/2}]^2$ and $[p_{1/2}]^2$ “coexistence” in the ^{10}He spectrum. We demonstrate that this problem has a key importance for understanding of observable properties of ^{10}He . We arrive to a conclusion that the simultaneous consistent understanding of the low-lying spectra of ^9He and ^{10}He is still a challenge both from theoretical and experimental sides.

The unit system $\hbar = c = 1$ is used in this work.

II. THEORETICAL MODEL

To choose the interactions in this work we generally follow the prescription of the three-cluster $^8\text{He}+n+n$ calculations of Ref. [5] with appropriate modifications of potentials. From the set of the core- n potentials tested in [5]

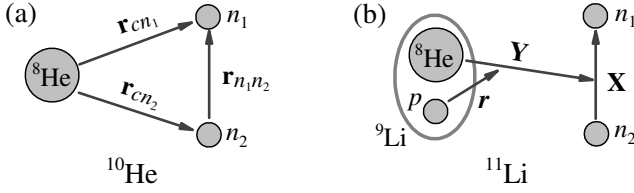


FIG. 1: Coordinate sets used in this paper. Panel (b) illustrates a proton removal from ^{11}Li as a method to populate ^{10}He .

we selected one (denoted there as “I2”). Other choices do not change qualitatively the result and quantitatively are quite close. The potential is parameterized by Gaussian formfactor

$$V_{c,ls}^l(r) = V_{c,ls}^l \exp[-r^2/r_0^2]$$

with $r_0 = 3.4$ fm. The depths of the d -wave potential $V_c^2 = -33$ MeV and the (ls) component in p -wave $V_{ls}^1 = 10$ MeV, are the same as in original paper. The inverse (ls) forces were used in Ref. [5] in p -wave to account for occupied $p_{3/2}$ subshell in the ^8He core. The interaction in the s -wave ^8He - n channel was pure repulsive in Ref. [5] to account for an occupied $s_{1/2}$ shell in the ^8He core. Central potential parameters in s - and p -waves V_c^0 and V_c^1 are being varied to clarify different aspects of the system dynamics. To manage the occupied $s_{1/2}$ state in ^8He in this work an additional repulsive core is introduced in the s -wave with parameters $r_0(\text{core}) = 2.35$ fm and $V_c^0(\text{core}) = 75$ MeV.

With the above potential the d -wave state in ^9He is found at 4.8 MeV which is consistent with the experimental data [3, 8, 12] giving values in the range 4.2–4.9 MeV for the $d_{5/2}$ state. With $V_c^1 = -10$ MeV (the value from the Ref. [5]) the $p_{1/2}$ state is obtained at 0.74 MeV. This value is different from value 1.15 MeV quoted in Ref. [5], where this is the energy at which the phase shift pass $\pi/2$. In this work we have to deal also with broad states, where the phase shift does not reach $\pi/2$. Thus, we define the resonance position for two-body subsystem by “observable value” (peak in the elastic cross section) and define the width as the full width on half maximum (FWHM) for this peak.

The realistic soft-core potential [13] is used in the n - n subsystem also following Ref. [5].

To study qualitatively a possible influence of the reaction mechanism we follow the approach of paper [14] to exotic ^5H system. We introduce a compact source function $\Phi(\rho, \Omega_\rho)$ in the right hand side of the three-body Schrödinger equation and solve the inhomogeneous system of equations

$$(\hat{H} - E) \Psi_E^{(+)}(\rho, \Omega_\rho) = \Phi(\rho, \Omega_\rho), \quad (1)$$

$$\begin{aligned} \hat{H} &= \hat{T} + \hat{V}_{cn}(\mathbf{r}_{cn1}) + \hat{V}_{cn}(\mathbf{r}_{cn2}) + \hat{V}_{nn}(\mathbf{r}_{n1n2}), \\ \rho^2 &= \frac{8}{10} (r_{cn1}^2 + r_{cn2}^2) + \frac{1}{10} r_{n1n2}^2 = \frac{1}{2} X^2 + \frac{8}{5} Y^2, \end{aligned} \quad (2)$$

for pure outgoing wave boundary conditions, utilizing the hyperspherical harmonic (HH) method. The used coordinates are shown in Fig. 1. The hyperradial components $\chi_{K\gamma}^{(+)}(\rho)$ of the WF

$$\Psi_E^{(+)}(\rho, \Omega_\rho) = \rho^{-5/2} \sum_{K\gamma}^{K_{\max}} \chi_{K\gamma}^{(+)}(\rho) \mathcal{J}_{K\gamma}^{JM}(\Omega_\rho),$$

are matched to Riccati-Bessel functions of half-integer index $\mathcal{H}_{K+3/2}^{(+)}$. Functions $\mathcal{H}^{(+)}$ have the asymptotic behavior $\exp[i\kappa\rho]$, where $\kappa = \sqrt{2ME}$ (M is a nucleon mass), describing the partial outgoing waves for hyperspherical equations. The value K_{\max} truncates the hyperspherical expansion. The hypermoment κ is expressed via the energies of the subsystems E_x , E_y or via Jacobi momenta k_x , k_y conjugated to Jacobi coordinates X , Y :

$$\begin{aligned} \mathbf{k}_x &= \frac{1}{2} (\mathbf{k}_{n1} - \mathbf{k}_{n2}), \quad \mathbf{k}_y = \frac{4}{5} (\mathbf{k}_{n1} + \mathbf{k}_{n2}) - \frac{1}{5} \mathbf{k}_c, \\ \kappa^2 &= 2ME = 2M(E_x + E_y) = 2k_x^2 + \frac{5}{8} k_y^2. \end{aligned} \quad (3)$$

The Jacobi variables are given in “T” Jacobi system. A more detailed picture of Jacobi coordinates for coordinate and momentum spaces in “T” and “Y” Jacobi systems can be found in Fig. 13.

The set of coupled equations for functions $\chi^{(+)}$ has the form

$$\begin{aligned} \left[\frac{d^2}{d\rho^2} - \frac{\mathcal{L}(\mathcal{L}+1)}{\rho^2} + 2M \{E - V_{K\gamma, K\gamma}(\rho)\} \right] \chi_{K\gamma}^{(+)}(\rho) \\ = 2M \sum_{K'\gamma'} V_{K\gamma, K'\gamma'}(\rho) \chi_{K'\gamma'}^{(+)}(\rho) + 2M \Phi_{K\gamma}(\rho), \end{aligned} \quad (4)$$

$$V_{K\gamma, K'\gamma'}(\rho) = \int d\Omega_\rho \mathcal{J}_{K'\gamma'}^{JM*}(\Omega_\rho) \sum_{i < j} V_{ij}(\mathbf{r}_{ij}) \mathcal{J}_{K\gamma}^{JM}(\Omega_\rho), \quad (5)$$

$$\Phi_{K\gamma}(\rho) = \rho^{5/2} \int d\Omega_\rho \mathcal{J}_{K\gamma}^{JM*}(\Omega_\rho) \Phi(\rho, \Omega_\rho),$$

where $\mathcal{L} = K + 3/2$ and $V_{K\gamma, K'\gamma'}(\rho)$ are matrix elements of the sum of the pairwise potentials referred to in this work as three-body potentials.

More detailed account of the method can be found e.g. in Ref. [14]. It is shown there that the method is consistent with “sudden removal” approximation for high energy fragmentation reactions. The development of the technically similar approach in the framework of the DWBA theory, applied to the inelastic processes in the transfer reactions, can be found in Ref. [15].

We used two different sources, consistent with different reaction conditions. One is a “narrow” source with a Gaussian formfactor

$$\Phi(\rho, \Omega_\rho) = \exp[-\rho^2/\rho_0^2] \sum_{K=0,2} \sum_{S=0} \mathcal{J}_{K\gamma}^{JM}(\Omega_\rho), \quad (6)$$

where $\rho_0 = 4.1$ fm provides the source rms radius $\langle \rho \rangle = 5$ fm. This is a typical radius for the “reaction volume” for

ordinary nuclei. The source populates only the lowest hyperspherical components of the WF ($K = 0, 2$). This qualitatively corresponds to the population of the $[s]^2$ and $[p]^2$ shell model configurations in the ^{10}He nucleus, which are expected to be the most important for the low-energy part of the spectrum. The condition $S = 0$ is qualitatively consistent with mechanism of transfer reactions, where the ^{10}He states are populated by transferring a two-neutron pair (with total spin equal zero) to the ^8He core. In such reactions the $\Delta S = 1$ transfer is strongly suppressed and the $\Delta S = 0$ transfer is a very reliable assumption.

The other choice of the source is more reaction specific. When ^{10}He is produced from ^{11}Li in a process which can be approximated as a sudden proton removal from ^9Li core, the source term $\Phi(\rho, \Omega_\rho)$ should contain the Fourier transform of the overlap integral between the ^8He WF $\Psi_{s\text{He}}$, the spin-isospin function of the removed proton χ_p and the ^{11}Li wave function over the radius-vector \mathbf{r} between the removed proton and the center-of-mass of ^{10}He [see Fig. 1 (b)]:

$$\Phi(\rho, \Omega_\rho) = \int d\mathbf{r} e^{i\mathbf{q}\mathbf{r}} \langle \Psi_{s\text{He}} \chi_p | \Psi_{^{11}\text{Li}} \rangle. \quad (7)$$

In general, this quantity is a complicated function of the recoil momentum vector \mathbf{q} , transferred to the ^{10}He system in the proton removal process. However, if the reaction energy is large and the internal energy of ^{10}He is small, one can neglect this dependence (see Ref. [14] for details). It can be shown that in this case partial hyperspherical components of the source function are well approximated by the corresponding components of the ^{11}Li WF. Thus, this type of calculations is further referred as “ ^{11}Li source”. The ^{11}Li WF was taken from an analytical parametrization developed in Ref. [16] taking into account broad range of experimental information on this nucleus. The dominant $[s_{1/2}]^2$ and $[p_{1/2}]^2$ configurations are populated by the ^{11}Li source with almost equal probabilities. The rms radius of such a source function $\langle \rho \rangle = 9.5$ fm is enormous compared to typical nuclear sizes.

In the approach with the source function of Eq. (1) the cross section for population of the ^{10}He continuum is proportional to the outgoing flux of the three particles on a hypersphere of some large radius $\rho = \rho_{\text{max}}$:

$$\frac{d\sigma}{dE} \sim \frac{1}{M} \text{Im} \int d\Omega_\rho \Psi_E^{(+)\dagger} \rho^{5/2} \frac{d}{d\rho} \rho^{5/2} \Psi_E^{(+)} \Big|_{\rho=\rho_{\text{max}}}. \quad (8)$$

Differentials of this flux on the hypersphere provide angular and energy distributions among the decay products at given decay energy E (see Ref. [14] for details of correlation calculations).

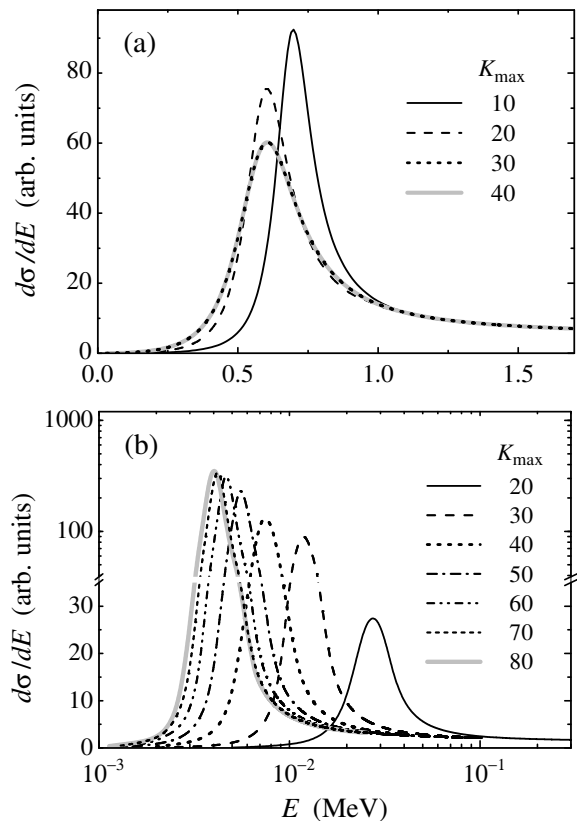


FIG. 2: Convergence of calculations as a function of K_{max} (the value truncating the hyperspherical basis). Calculations with narrow source. (a) Resonance peak with $[p_{1/2}]^2$ structure. The ^8He - n potential parameters are: $V_c^0 = 0$, $V_c^1 = -10$ MeV. (b) Resonance peak with $[s_{1/2}]^2$ structure. Parameters are: $V_c^0 = -26.93$ MeV (this corresponds to $a = -15$ fm in ^9He), $V_c^1 = -4.5$ MeV.

III. CALCULATIONS

A. Basis size convergence

The HH calculations in our method can be performed with $K_{\text{max}} = 24 - 26$. Such basis sizes could be not sufficient for obtaining a good energy convergence of calculations in some complicated cases. The basis size can be further increased effectively using the adiabatic procedure based on the so called Feshbach reduction (FR) [17]. Feshbach reduction eliminates from the total WF $\Psi = \Psi_p + \Psi_q$ an arbitrary subspace q using the Green's function of this subspace:

$$H_p = T_p + V_p - V_{pq} G_q V_{pq}.$$

In a certain adiabatic approximation we can assume that the radial part of kinetic energy is small under the centrifugal barrier in the channels with high centrifugal barriers and can be approximated by a constant. In this approximation the FR procedure is reduced to the construction of effective three-body interactions $V_{K\gamma, K'\gamma'}^{\text{eff}}$ by

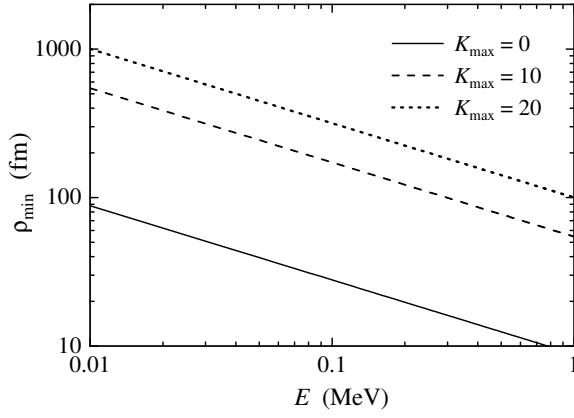


FIG. 3: Hyperradius of the classical turning point ρ_{\min} for hyperradial centrifugal barriers in the channels with different K values.

matrix operations

$$G_{K\gamma, K'\gamma'}^{-1} = (H - E)_{K\gamma, K'\gamma'} = V_{K\gamma, K'\gamma'} + \left[E_f - E + \frac{(K + 3/2)(K + 5/2)}{2M\rho^2} \right] \delta_{K\gamma, K'\gamma'},$$

$$V_{K\gamma, K'\gamma'}^{\text{eff}} = V_{K\gamma, K'\gamma'} - \sum V_{K\gamma, \bar{K}\bar{\gamma}} G_{\bar{K}\bar{\gamma}, \bar{K}'\bar{\gamma}'} V_{\bar{K}'\bar{\gamma}', K'\gamma'}.$$

Summation over indexes with bar is made for eliminated channels. We take the “Feshbach energy” E_f in our calculations as $E_f \equiv E$.

Reliability of the FR procedure can be checked in two ways. We can compare dynamic calculations for some large K_{\max} with the “reduced” calculations $K_{\max} \rightarrow K_{FR}$ (with much smaller dynamic basis size K_{FR}) and in principle they should coincide. Calculations show that for ^{10}He starting from $K_{\max} = 26$ we get practically the same result down to $K_{FR} = 10$. The other way to make a check is the following. We can also start FR with some quite large fixed K_{\max} (e.g. from $K_{\max} = 100$ in this work), make the reduction to different $K_{FR} \leq 26$ and perform dynamic calculations with each of them. Again the results were found to coincide precisely for $K_{FR} \geq 10$. Thus it was found reliable to perform most of the calculations (except those for correlations) with dynamic basis size $K_{FR} = 12$ varying effective basis size K_{\max} when necessary.

The cross section convergence with the increase of the effective hyperspherical basis size is demonstrated in Fig. 2. For resonance peak with $[p_{1/2}]^2$ structure the convergence is reliably achieved by $K_{\max} = 30$. However, in the case of a state with $[s_{1/2}]^2$ structure more efforts are required to achieve the convergence (very close to the threshold even a minor variation of the energy becomes noticeable). We intentionally demonstrate in Fig. 2 (b) the case, which is numerically more complicated than the others considered in the paper. When the s -wave potential in the ^8He - n subsystem is taken to provide the scattering length $a = -15$ fm, the resonance peak in ^{10}He is obtained at $E = 4$ keV with $\Gamma = 0.7$ keV. The basis

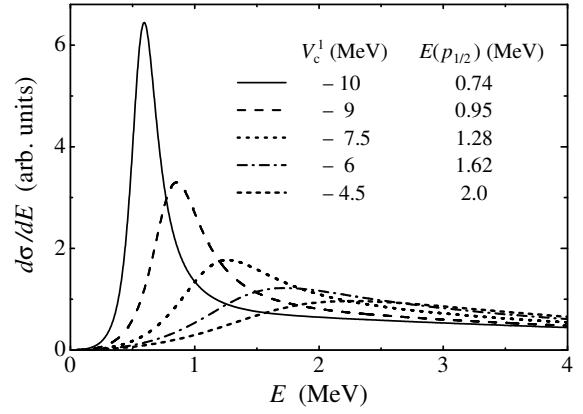


FIG. 4: Behavior of the ^{10}He spectrum with decrease of the p -wave potential depth V_c^1 . The corresponding $p_{1/2}$ state energies $E(p_{1/2})$ in ^9He relative to the ^8He - n threshold are shown in the legend. Calculations with narrow source.

size $K_{\max} = 80$ is required in such a case to obtain the convergence.

Another aspect of the basis size choice is connected with the radial extent of the calculations ρ_{\max} . The formulation of the cross section calculations in the form (8) implies that the WF residues at ρ_{\max} in the classically allowed region. Taking into account the character of the hyperspherical centrifugal barrier (4) this requires a very large radial extent for large basis sizes. Fig. 3 provides the estimates of the minimally required values of ρ_{\max} to satisfy this condition for different K values. So, we used $\rho_{\max} \sim 300 - 500$ fm for calculations of the $[p_{1/2}]^2$ states and $\rho_{\max} \sim 1000 - 2000$ fm for the extreme low-energy calculations of the $[s_{1/2}]^2$ states.

B. Sensitivity to the p -wave in ^9He

The ground state resonance properties were predicted as $E \sim 0.7 - 0.9$ MeV, $\Gamma \sim 0.1 - 0.3$ MeV in Ref. [5]. Within the approach used in this work we first of all reproduce the results of previous studies. The calculation with model parameters consistent with these of Ref. [5] is shown in Fig. 4, by solid curve. The peak position is somewhat lower than in Ref. [5] ($E = 0.6$ MeV, $\Gamma = 0.27$ MeV) which is connected to the larger basis size (see Fig. 2(a)). Note that $K_{\max} = 8$ was used in Ref. [5].

The evolution of the cross section with decrease of the p -wave interaction from the value adopted in Ref. [5] ($V_c^1 = -10$ MeV, which provided the energy of the $p_{1/2}$ state $E(p_{1/2}) = 0.74$ MeV) to a value providing the ^9He g.s. to be at about 2 MeV ($V_c^1 = -4.5$ MeV), is shown in Fig. 4 for the narrow source function. The new peak position for the ^{10}He population cross section is at $E = 2.3$ MeV. The impact of this change is drastic: the narrow ^{10}He g.s. peak is practically “dissolved” as the system becomes less bound: e.g. the width of the peak can not be any more well defined as FWHM.

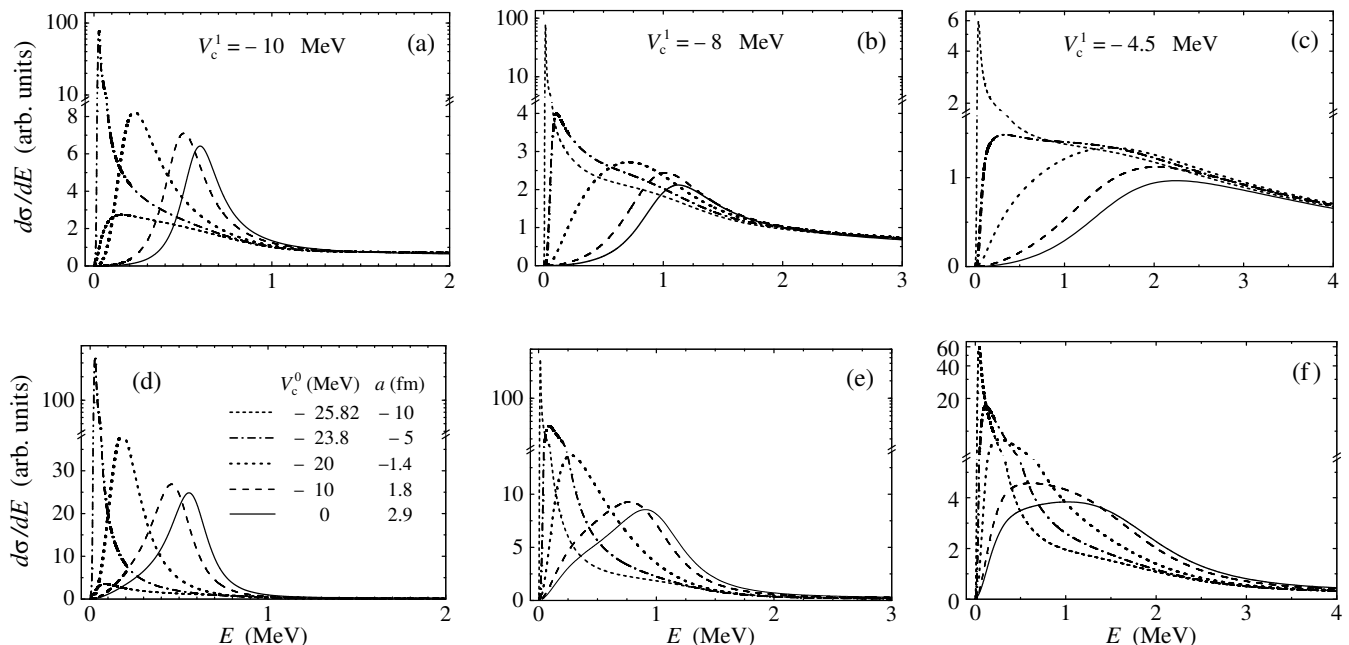


FIG. 5: Behavior of the ^{10}He spectrum with increase of the s -wave interaction [legend, the same for all panels is shown in panel (d)]. The first row shows the narrow source case, the second row is for broad (^{11}Li) source. In the first column calculations for p -wave potential $V_c^1 = -10$ MeV ($p_{1/2}$ state at 0.74 MeV, as in calculations of Ref. [5]); in the second column for $V_c^1 = -8$ MeV ($p_{1/2}$ state at 1.16 MeV, close to 1.27 MeV, as in experiment [8]); in the third column for $V_c^1 = -4.5$ MeV ($p_{1/2}$ state at 2 MeV, as in experiment [12]). Smooth behavior of the short-dashed curves ($V_c^0 = -25.82$ MeV, $a = -10$ fm) in panels (a) and (d) is connected to the fact that the bound 0^+ state of ^{10}He is formed with binding energy ≈ 60 keV. Note, the change of the scales on the vertical axes to logarithmic.

C. Sensitivity to the reaction mechanism

The evolution of cases with different p -wave interactions with increase of the s -wave interaction is shown in Fig. 5 for the narrow and broad source functions, which should simulate different reaction conditions. We first discuss sensitivity of the cross section to the reaction mechanism.

The narrow ground state in ^{10}He is not significantly sensitive to the reaction mechanism. This can be seen comparing Figs. 5 (a) and (d): difference of curves of the same style in the upper and lower panels is quantitative, not qualitative. This is an expected result as the narrow states have a sufficiently large lifetime to “forget” how they were populated and thus loose the sensitivity to the population mechanism.

When the state is above 1 MeV, the width becomes comparable to 1 MeV and the dependence on the source function is considerable [Figs. 5 (b) and (e)]. In the case of even higher ^{10}He g.s. the calculations with narrow and broad sources have very little in common [Figs. 5 (c) and (f)]. According to the recent result [12] the cases (c) and (f) should be regarded as the most realistic. Thus peculiarities of the reaction mechanism could be a problem for interpretation of the ^{10}He spectra.

D. Sensitivity to the s -wave in ^9He

It can be seen from Fig. 5 that for relatively weak s -wave attraction the g.s. peak is shifted to lower energies with minimal distortion. However, as the s -wave attraction becomes stronger the threshold peculiarity is formed in the spectrum. With the further increase of the s -wave interaction this peculiarity is transformed into very sharp low-energy ($E < 300$ keV) peak. The WF at this peak has a practically pure $[s_{1/2}]^2$ structure and we characterize it as a “three-body virtual state”.

Using the term “three-body virtual state” we have two things in mind: this is an s -wave state build upon the virtual states in all the subsystems, and this state has distinct properties compared to ordinary resonant three-body states (relevant discussion of “Efimov-like three-body virtual excitations” can be found in Ref. [18]).

The ordinary two-body virtual states are typically characterized in two ways: (i) as a negative energy pole on the second Riemann sheet or (ii) as a threshold peculiarity [37] preceding the formation of the bound state in the case of absence of the potential barrier. The pole behavior in the three-body systems has been studied in a number of works with the emphasis on the possible similarities with two-body virtual state poles behavior [11, 19, 20, 21, 22]. In paper [22] the possibility of such behavior in the three-body s -wave system was shown for

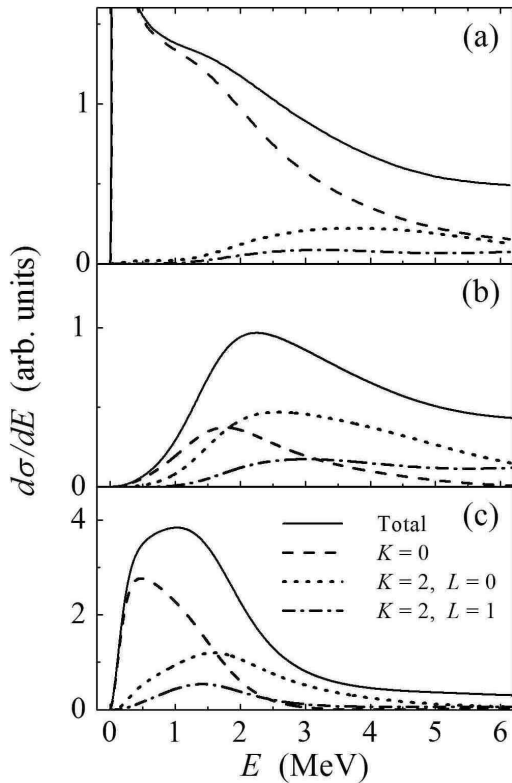


FIG. 6: Partial decomposition of the cross section; dashed, dotted and dash-dotted curves provide contributions of the main WF components. Calculations with p -wave resonance in ${}^9\text{He}$ at 2 MeV ($V_c^1 = -4.5$ MeV). Different panels correspond to: (a) $V_c^0 = -25.82$ ($a = -10$ fm), narrow source; (b) $V_c^0 = 0$ narrow source, and (c) $V_c^0 = 0$, ${}^{11}\text{Li}$ source.

interactions with certain extreme properties. Observable consequences of such a pole behavior in the three-body systems remain unclear. Our way to think about three-body virtual state is more relevant to the second characteristic of the two-body virtual state, which is connected to its observables.

For relatively strong s -wave interaction in the ${}^8\text{He}$ - n subsystem (namely such that the scattering length $a < -5$ fm), we unavoidably (means independently on the structure and reaction mechanism details) get a sharp peak in the cross section with energy less than 0.3 MeV and with dominating $[s_{1/2}]^2$ configuration. Stable formation of the low-energy peak at certain strength of attractive s -wave interaction in ${}^9\text{He}$ is an important dynamical feature of the ${}^{10}\text{He}$ system which makes us optimistic about predictive abilities of theoretical models in this situation. The extreme low-energy peaks could hardly be consistent with the experimental data [6], the discussion of the issue is provided below in Section IV A.

It can be noticed that in the case of the very narrow three-body virtual state formation, some structure can be seen as a “shoulder” on the right slope of the $[s_{1/2}]^2$ peak. It is possible to understand that this structure corresponds to the state with the $[p_{1/2}]^2$ structure which

becomes sufficiently well split from the $[s_{1/2}]^2$ state and even preserves the position typical for $V_c^0 = 0$ case. The analysis of the partial decomposition of the cross section provided in Fig. 6 indicates that this is generally true. However, the $[p_{1/2}]^2$ contribution to WF is considerably broadened and reduced in absolute value compared to the case when there was no s -wave attraction. For understanding of Fig. 6 it is useful to note that at the “shell model language” the $K = 0$ configuration is a pure $[s_{1/2}]^2$, while the $K = 2$ components (for p -shell nuclei) are mainly decomposed as

$$\begin{aligned} |K = 2, L = 0\rangle &= \sqrt{1/3} [p_{1/2}]^2 + \sqrt{2/3} [p_{3/2}]^2, \\ |K = 2, L = 1\rangle &= \sqrt{2/3} [p_{1/2}]^2 - \sqrt{1/3} [p_{3/2}]^2. \end{aligned}$$

The weight of the $[p_{1/2}]^2$ configuration relative to the total weight of $[p_{1/2}]^2$ and $[p_{3/2}]^2$ configurations varies from 80 to 90 percent in different calculations of the p -wave state.

E. Properties of the three-body virtual state

Important feature which differs a three-body virtual state (the one with dominant $[s_{1/2}]^2$ structure) from the ordinary two-body virtual states is evident from the structure of equations (4). This feature has been exploratory discussed in the past (e.g. Ref. [20]), but it seems that in ${}^{10}\text{He}$ this kind of physics could become really accessible for observation. The state with $[s_{1/2}]^2$ structure should be characterized by domination of component with lowest possible value of the generalized angular momentum $K = 0$. However, the centrifugal barrier $\mathcal{L}(\mathcal{L} + 1)/2M\rho^2$ is not zero even in the channel with $K = 0$, as it depends on “effective angular momentum” $\mathcal{L} = K + 3/2$. This means that the low-energy three-body virtual state may exist in the form of a real resonance peak, not a threshold peculiarity as two-body virtual state. It is also easy to demonstrate that the low-energy behavior of the inelastic cross section for population of the three-body continuum is

$$d\sigma/dE \propto E^2,$$

in contrast with the two-body inelastic cross section which has a square root peculiarity in the case of the virtual state

$$d\sigma/dE \propto \sqrt{E}.$$

Such a behavior should in principle distinctly separate the three-body virtual state peak from zero energy. Such a separation was demonstrated in Ref. [20] for a toy model of the $[s^2]$ state for the “Borromean system” [38]. Namely, it was shown in the analytical continuation of coupling constant (ACCC) method that the pole trajectories in the case of the $[s^2]$ three-body state are analogous to the trajectories in the system with barriers, while

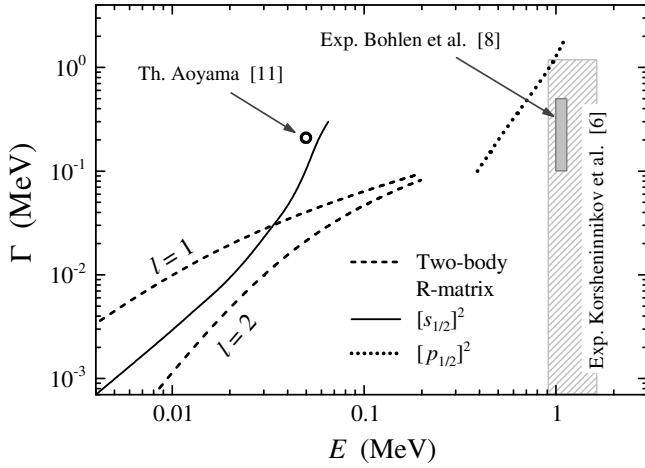


FIG. 7: Width as a function of resonance energy for $[s_{1/2}]^2$ and $[p_{1/2}]^2$ states. Standard two-body R-matrix estimates are shown for $l = 1$ and $l = 2$ (channel radius 40 fm) by dashed curves. Possible experimental ranges according to experiments [6, 8] are shown by hatched and grey rectangles correspondingly. The result of theoretical prediction [11] is shown by a small circle. The curve for $[p_{1/2}]^2$ state is calculated with the broad source. Calculations for $[s_{1/2}]^2$ state with broad and narrow sources practically coincide within the shown energy range.

for the two-body virtual states they are qualitatively different.

The mentioned features, however, do not mean that a three-body virtual state is an ordinary resonance state; there is an important difference. It is known that the resonance behavior is connected to time delays in the propagation of particles (and corresponding time-dependent theory can be formulated in these terms). Ordinarily, the time delay is connected to the confinement of particles inside the potential barrier and their WF is localized inside the potential well, displaying the “quasibound” nature of such resonances. In the case of virtual state the time delay is not connected with barrier and tight spacial localization of particles close to each other. It is connected with *slow* motion of particles in the volume of sphere with *large* radius (comparable to scattering length). In the three-body case the hyperspherical centrifugal barrier $\mathcal{L}(\mathcal{L} + 1)/2M\rho^2$ has an effective collective nature; it is clear that individual nucleons in $[s_{1/2}]^2$ configuration do not “see” any barriers. The time delay is connected therefore to the simultaneous presence of two valence nucleons in the volume around the core, associated with scattering lengths, which means a peripheral nature of such a state.

The peripheral character of the state presumes different character of the dependence of the resonance width on energy than the behavior which could be expected for “typical” barrier penetration. We can take, for example, the calculated properties of the ^{10}He g.s. in the case $a = -15$ fm ($E = 4$ keV, $\Gamma = 0.7$ keV, see Fig. 2) and deduce the “channel radius” ρ_{ch} using for penetra-

tion expression analogous to the single-channel R-matrix formula. It can be found in Ref. [24]:

$$\Gamma = \frac{1}{M\rho_{\text{ch}}^2} \frac{2}{\pi} \frac{1}{J_{K+2}^2(\kappa\rho_{\text{ch}}) + N_{K+2}^2(\kappa\rho_{\text{ch}})} . \quad (9)$$

Then the value $\rho_{\text{ch}} \approx 40$ fm is obtained. So, the radial range, which can be interpreted as an “internal region” in the case of the virtual three-body state, is huge.

The dependence of the width (defined as FWHM) on resonance energy is shown in Fig. 7 for $[s_{1/2}]^2$ and $[p_{1/2}]^2$ resonance peaks. The variation of energy in each case is obtained by respective variation of parameters of the s - and p -wave interactions. The $[p_{1/2}]^2$ curve is obtained in calculations with a broad source. The curves for $[s_{1/2}]^2$ calculations practically coincide for broad and narrow source calculations; this independence is an expected result for such a narrow structure. It can be seen in Fig. 7 that the curve for $[s_{1/2}]^2$ state stays mainly in between standard two-body R-matrix estimates with $l = 1$, $l = 2$ (channel radius 40 fm) as an “effective angular momentum” for $K = 0$ is $\mathcal{L} = 3/2$. The obtained dependence is in a good agreement with the ^{10}He ground state prediction by Aoyama [11] which gave $E = 0.05$ MeV and $\Gamma = 0.21$ MeV (small circle in Fig. 7). We think that this agreement is an important fact demonstrating stability of the theoretical results on this issue because very different theoretical models and different p -wave interactions were employed in the studies of Ref. [11].

The point about a peripheral character of the $[s_{1/2}]^2$ state is also confirmed by analysis of the correlation density. The correlation densities $|\Psi^{(+)}|^2$ for the ^{10}He WFs on the $\{\rho, \theta_\rho\}$ plane are shown in Fig. 8. The θ_ρ hyperspherical variable describes the distribution between X and Y subsystems. It is a component of the 5-dimensional hyperangle $\Omega_\rho = \{\theta_\rho, \Omega_x, \Omega_y\}$. For ^{10}He in the “T” Jacobi system

$$X = \sqrt{2}\rho \sin \theta_\rho \quad ; \quad Y = \sqrt{5/8}\rho \cos \theta_\rho .$$

Some properties of the three-body virtual state are well illustrated by this plot.

1. The $[s_{1/2}]^2$ and $[p_{1/2}]^2$ configurations demonstrate very different correlations in the internal region and on asymptotic. While in the $[s_{1/2}]^2$ case the distributions are expectedly quite featureless, in the $[p_{1/2}]^2$ case we observe in the internal region the double-humped structures — “dineutron” and “cigar” — in the variable θ_ρ , which are connected to so called Pauli focusing [Fig. 8 (b), (c); in the case (b) only “dineutron” peak is seen]. These structures are well known from the studies of the other p -shell nuclei [26]. In the case when there is no attractive s -wave interaction in the $^8\text{He}-n$ channel [Fig. 8 (c)] this double-humped correlation “survives” up to the asymptotic region in somewhat modified form and thus could possibly be observed in experiment (see also the discussion in the Section IV B).

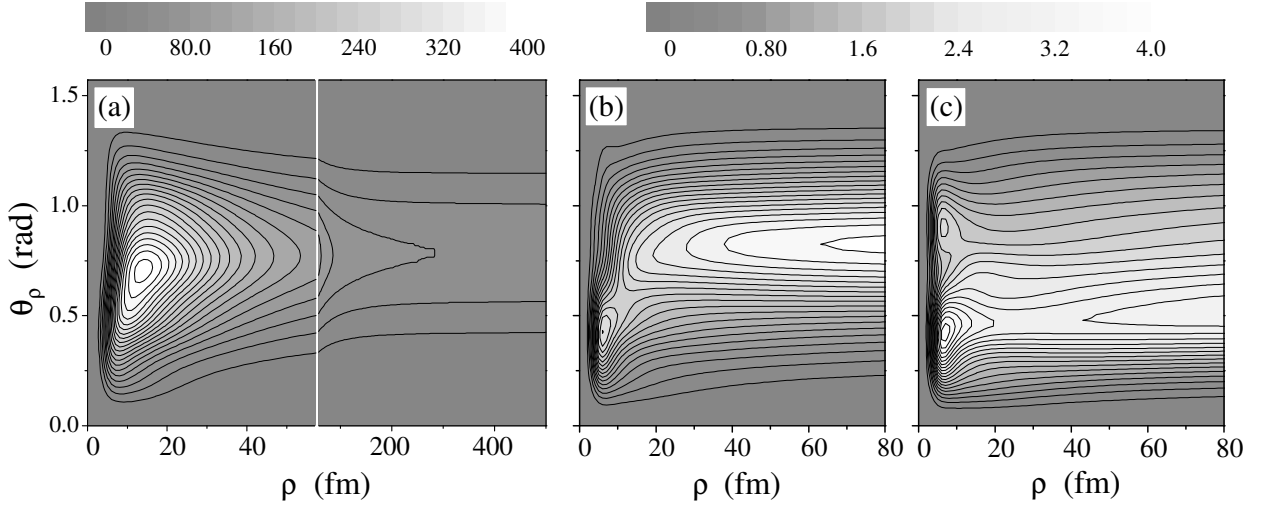


FIG. 8: Correlation density $|\Psi^{(+)}|^2$ for the ^{10}He WF on the $\{\rho, \theta_\rho\}$ plane in the “T” Jacobi system. Panel (a) shows case of strong three-body virtual state $V_c^0 = -26.93$ ($a = -15$ fm), $V_c^1 = -4.5$ MeV for energy taken on peak position ($E = 4$ keV). See also Fig. 2 (b). Panel (b) gives the same as (a) but for $E = 2.3$ MeV (the latter energy is the expected position for peak in the case of state with $[p_{1/2}]^2$ structure). Panel (c) shows the state with $[p_{1/2}]^2$ structure $V_c^0 = 0$, $V_c^1 = -4.5$ MeV. Calculations are made with narrow source; energy is taken on peak position ($E = 2.3$ MeV).

- Peripheral character of the $[s_{1/2}]^2$ WF. It can be seen from a comparison of Figs. 8 (b) and (c) that the double-humped structure connected to $[p_{1/2}]^2$ configurations is sharply concentrated in the internal region ($\rho \sim 7$ fm) and rapidly decreases beyond 10–15 fm. In contrast, the $[s_{1/2}]^2$ WF is peaked at $\rho \sim 15$ fm and extends smoothly to around 50 fm [Fig. 8 (a)]. Distance $\rho \sim 15$ is well beyond the typical nuclear size; for configurations with such typical ρ values the individual valence nucleons have on average 10 fm distance to the core.
- Radial stabilization of the $[s_{1/2}]^2$ WF (the distances at which the $\sim \exp[i\kappa\rho]$ behavior is mainly achieved) is taking place at quite large distances [$\rho \approx 300 - 400$ fm, see Fig. 8 (a)]. This is connected both to very low energy of the peak (4 keV in this particular calculation) and effectively long-range character of interactions in the s -wave ^8He - n channel, responsible for the formation of the three-body virtual state.
- One can see from Fig. 5 (c) that the cross section behavior in the energy region of $[p_{1/2}]^2$ state ($E \approx 2 - 3$ MeV) is practically not sensitive to the low-energy behavior of the spectrum (presence or absence of the $[s_{1/2}]^2$ state). It is thus possible to think that these configurations are practically independent in this energy region. A comparison of Figs. 8 (b) and (c) shows that this is not true. Both the internal structure of the WF and correlations for decay products demonstrate strong sensitivity to the presence of $[s_{1/2}]^2$ state, although it is not clearly seen in the total production cross section in this energy range.

An important technical insight could be obtained from the behavior of the effective hyperspherical interactions (5). In Fig. 9 we show the “most attractive” diagonal potential (this appear to to be $K = 0$ term in all the cases) and the lowest diagonalized potential. The later can be considered as an effective interaction for some simple adiabatic approximation to the problem, which is qualitatively illustrative, but quantitatively could be not very reliable. The important dynamical aspects which become clear from these plots have already been discussed in our work [14] on example of broad states of ^5H system. It can be seen in Fig. 9 that even the “most attractive” diagonal potentials are in reality repulsive and do not even show any sign of “pocket” formation. The structures in the continuum are formed here only by interaction of multiple channels. It is interesting to note that the possibility of this class of states has been discussed many years ago (so called “resonances of the second kind” [25]) but now we seem to face them systematically in the few-body dripline nuclei.

In the broad range of the resonance energies the state is located above the effective barrier top. Formation of the peaks, which could be very narrow (see Figs. 5, 7) is presumably connected here not with barrier penetration, but with slow motion above the barrier and reflection from the right slope of the barrier [39]. Only in the extreme low energy case Fig. 9 (c) the process could be interpreted as penetration through the effective barrier. Typical range of the barrier is consistent in this case with the “channel radius” estimates by Eq. (9).

The evolution of the nuclear structure near the threshold is also an interesting question which is briefly discussed below. The short-dash curves ($V_c^0 = -25.82$ MeV, $a = -10$ fm) in Fig. 5 (a) and (d) show qualitatively dif-

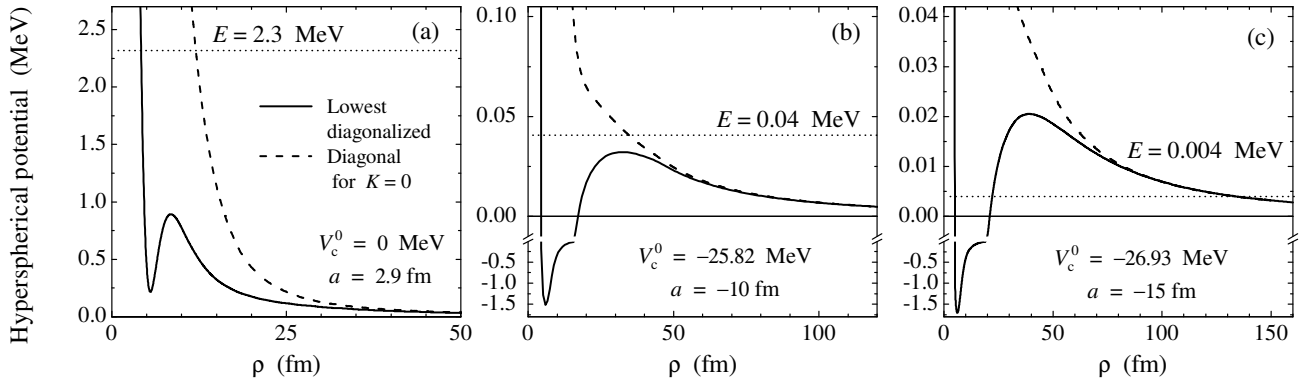


FIG. 9: Hyperspherical potentials (5) as function of hyperradius. Solid line shows the lowest diagonalized potential, dashed line shows the lowest diagonal potential (in all the cases this is $K = 0$ term). (a) The $[p_{1/2}]^2$ state at $E = 2.3$ MeV [see solid curves in Fig. 5 (c), (f)]. Panels (b) and (c) correspond to $[s_{1/2}]^2$ states at $E = 0.04$ MeV [see short-dashed curves in Fig. 5 (c), (f)] and at $E = 0.004$ MeV respectively.

ferent behavior compared to the expected sharpening of the threshold peak. It happens because in this case the bound 0^+ state of ^{10}He is formed with binding energy ≈ 60 keV. Therefore these curves do not represent a valid result in the context of our studies (we should consider only the three-body Hamiltonians which do not lead to the bound ^{10}He). However, it is interesting to see how the nuclear structure evolves in this case (Table I). The virtual three-body state shows strong domination of the $[s_{1/2}]^2$ component in the internal region (the first row in Table I). As soon as the state becomes bound, the structure changes drastically with rapid increase of the $[p_{1/2}]^2$ configuration weight (see the second row from Table I). If we bind the ^{10}He even more strongly, so that the binding energy becomes 0.3 MeV, which corresponds to the binding energy of ^{11}Li , its structure begins to resemble closely the typical structure of ^{11}Li with practically equal population of the $[s_{1/2}]^2$ and $[p_{1/2}]^2$ configurations (the third row in Table I). So, the bound analogue of the virtual three-body state is expected to be not a state with dominant $[s_{1/2}]^2$ configuration, but a state with strong “competition” between the s -wave and p -wave configurations. Usually the structure of narrow resonant (or quasi-bound) states is characterized by a high identity with the structure of the corresponding bound states [40]. The virtual three-body state demonstrates the behavior, which is qualitatively different in this respect.

Based on the presented results we can probably conclude that in the sense of nuclear dynamics the three-body virtual states are something intermediate between two-body virtual state and an ordinary resonance.

F. Consistence with $3 \rightarrow 3$ scattering calculations

The model cross section calculations for realistic ^9He energies Fig. 5 (c) and (f) show very diverse results in the case of narrow and broad sources. A question can be asked in that case what should be considered as a “real”

position of ^{10}He g.s. and whether it is reasonable at all to speak about such “real” position if diverse experimental responses could be expected. The theoretical approach which is “neutral” with respect to possible reaction mechanism is represented by $3 \rightarrow 3$ scattering calculations.

Figures 10 and 11 show the results of the $3 \rightarrow 3$ scattering calculations in the cases of a pure $[p_{1/2}]^2$ state and the same in the presence of the low-energy $[s_{1/2}]^2$ state respectively. The details of the approach can be found in Ref. [27] on example of the ^5H nucleus. Three-body Hamiltonian here is the same as in Figs. 5 (c) and (f). Three different values are displayed for these calculations: the diagonal $3 \rightarrow 3$ scattering phase shifts, the first diagonalized phase shift (so called eigenphase), and the diagonal internal normalizations for scattering WFs

$$N_{\rho_{\text{int}}}(E) = \frac{1}{\mathcal{V}^5} \sum_{K\gamma} \int_0^{\rho_{\text{int}}} d\rho \left| \chi_{K\gamma}^{K\gamma}(\mathcal{V}\rho) \right|^2. \quad (10)$$

The size of the “internal region” $\rho_{\text{int}} = 6$ fm was taken for this value as in Ref. [27].

For $[p_{1/2}]^2$ state the $3 \rightarrow 3$ calculations in Fig. 10

TABLE I: Internal structure of the virtual three-body state and the bound ^{10}He states close to the $^8\text{He}+n+n$ threshold.

E (MeV)	$[s_{1/2}]^2$	$[p_{1/2}]^2$	$[p_{3/2}]^2$	$[d]^2$
0.04 ^a	93.3	2.2	1.8	1.8
-0.06 ^b	66.1	23.8	4.7	4.2
-0.3 ^c	51.0	35.9	6.1	5.7

^aCalculation of Fig. 5 (c), short-dashed curve ($V_c^0 = -25.82$ MeV, $a = -10$ fm, $V_c^1 = -4.5$ MeV). Radius for internal normalization was taken $\rho_{\text{int}} = 40$ fm, see Fig. 8 (a).

^bContinuum above this bound state is shown in Figs. 5 (a) and (d) by the short-dashed curves ($V_c^0 = -25.82$ MeV, $a = -10$ fm, $V_c^1 = -10$ MeV).

^cThe same calculation as ^b, but with extra binding added by attractive three-body potential.

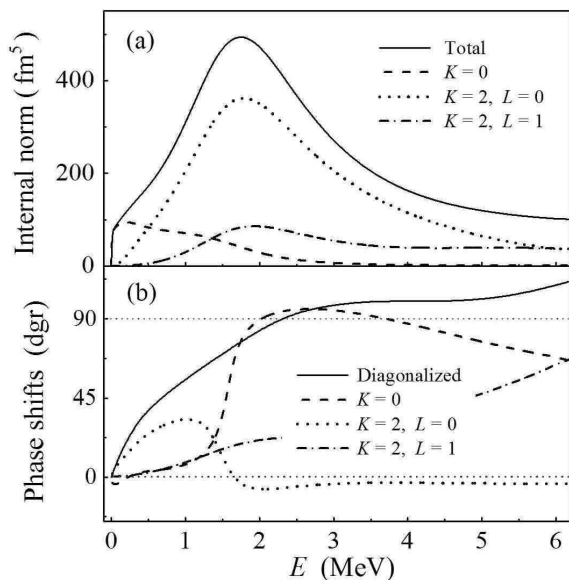


FIG. 10: The $3 \rightarrow 3$ scattering calculations, $V_c^0 = 0$, $V_c^1 = -4.5$ MeV. (a) Internal normalizations Eq. (10) for dominant components of the WF. (b) Diagonalized phase shift (“eigenphase”) is shown by solid curve, while diagonal phase shifts for the lowest hyperspherical components are given by dashed, dotted, and dash-dotted curves.

give somewhat different resonant energies for different responses: $E = 1.8$ MeV for internal normalization, $E \sim 2$ MeV for the most strongly changing diagonal phase shifts and $E = 2.3$ for eigenphase. Such spread is clearly connected to the fact that the phase shifts barely pass 90 degrees. So, we can speak about resonant energy of about $E \sim 2.0 - 2.3$ MeV, when only scattering is concerned. The agreement of $3 \rightarrow 3$ calculations with narrow source calculations is reasonable. That could be an indication that “ordinary” reactions (simulated in this model) are a preferable tool to access properties of ^{10}He compared to reactions with exotic nuclei (like ^{11}Li).

In the case of narrow low-lying $[s_{1/2}]^2$ state (shown in Fig. 11) the results provided by all $3 \rightarrow 3$ calculations (resonance energy $E = 40$ keV) are in excellent agreement with each other and with previous model calculations [Fig. 5 (c) and (f), curves with $a = -10$ fm]. This state is formed exclusively by $K = 0$ WF component. An evidence for the $[p_{1/2}]^2$ state contributions could be found in the phase shift at around 2 MeV, but it is not very expressed. Better evidence is provided by internal normalizations for $K = 2$ components of the WF. These show maximum at about 2.3 MeV and provide much broader structures, than in the case of the $[p_{1/2}]^2$ state not affected by $[s_{1/2}]^2$ configuration (Fig. 10). Again, we can come to a conclusion that the $[p_{1/2}]^2$ state survives in the presence of the $[s_{1/2}]^2$ state in somewhat modified (shifted up and broadened) form, but the population of it is expected to be poor.

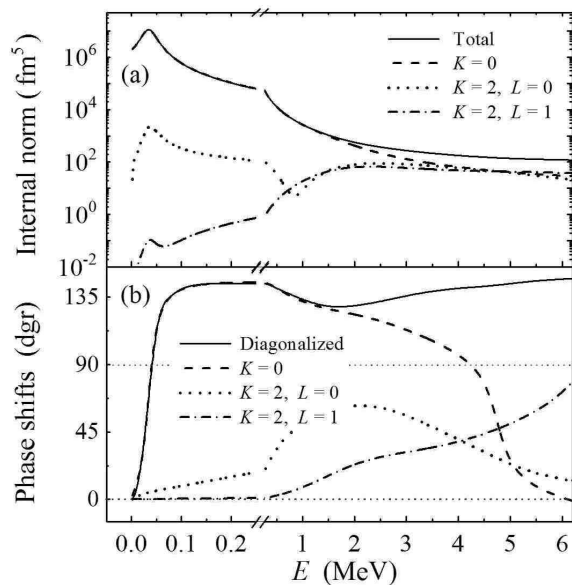


FIG. 11: The $3 \rightarrow 3$ scattering calculations, $V_c^0 = -25.82$ MeV ($a = -10$ fm), $V_c^1 = -4.5$ MeV. See Fig. 10 for details.

IV. DISCUSSION

A. What is the ground state of ^{10}He ?

It was proposed in Ref. [11] that the observed so far state of ^{10}He is not the ground but the first excited state with $[p_{1/2}]^2$ structure while the ground $[s_{1/2}]^2$ state remains unobserved. We confirm here the finding of Ref. [11] that for considerable s -wave attraction in ^9He subsystem two 0^+ states with different structures should coexist in the low-energy spectrum of ^{10}He . However, we also find that population of the $[s_{1/2}]^2$ configuration (in the case of a strong s -wave attraction in ^9He and realistic reaction scenario) is always very pronounced compared to the $[p_{1/2}]^2$ configuration. For that reason we can expect that if the $[s_{1/2}]^2$ state *really exists* then the $[p_{1/2}]^2$ component is difficult to observe in experiment (as it is lost on a “nonresonant background” of $[s_{1/2}]^2$ low-energy excitation). It can be found that the energy position of the $[p_{1/2}]^2$ component of 0^+ state is quite stable when the s -wave attraction is increased. However, for extreme cases of the s -wave attraction this contribution becomes much broader and in general “lost” on a thick right “tail” of the $[s_{1/2}]^2$ ground state.

Current experimental situation in ^{10}He is clearly not in favour of the $[s_{1/2}]^2$ state existence. Several theoretical spectra of ^{10}He are provided in Fig. 12 on top of the experimental data Ref. [6]. Theoretical curves are convoluted with energy resolution of the experiment [6] which is parameterized as $\Delta E = 0.7\sqrt{E}$ (ΔE is FWHM). The calculation with ^9He subsystem having $p_{1/2}$ g.s. at about 2 MeV reasonably fit the data. The experimental cross section peaked at about 1.2 MeV could be consistent with

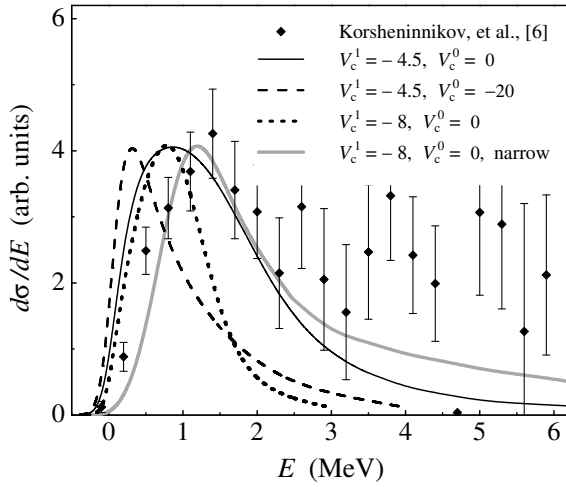


FIG. 12: Calculation results convoluted with experimental resolution of Ref. [6] and experimental data. Solid, dashed, and dotted curves correspond to calculations with ^{11}Li source [see Fig. 5 (f) solid, (f) dotted, and (e) solid curves]. Gray line shows calculation with narrow source [Fig. 5 (b) dotted curve].

some range of p -wave interactions for ^{11}Li source [Fig. 5, (e)–(f)]. This, however, is possible only for quite a weak attractive part of s -wave potential: $V_c^0 > -20$ MeV. For such value of parameters the s -wave interaction is in general still effectively repulsive (due to a large repulsive core). For that reason, if we completely rely on the data [6] we would impose theoretical limit $a > -5$ fm for ^8He - n scattering length. The derived theoretical limit is in a strong contradiction with the *upper* limit for scattering length in ^9He $a < -10$ fm imposed in experiment [10]. There is no contradiction between our theoretical limit and data [12] where a *lower* limit $a > -20$ fm for scattering length is given.

The unclear situation with exotic reaction mechanism expected for reactions with ^{11}Li could have been resolved by a different experimental approach. Such an experiment in principle exists: the ground state of ^{10}He and two excited states were identified in the complicated $2p$ - $2n$ exchange reaction $^{10}\text{Be}(^{14}\text{C}, ^{14}\text{O})^{10}\text{He}$ [7, 8]. Unfortunately, the observed peaks rest on a “thick” background and has a low statistical confidence. None of our calculations are consistent with the results of this experiment. Namely, we can not reproduce in any model assumptions the small width of the g.s. obtained in this work (300 ± 200 keV at 1.07 MeV of excitation). For example, in Fig. 5 (b) the width of the state found at about 1.1 MeV is $\Gamma \sim 1.1$ MeV (see also Fig. 7). Smaller width of the ^{10}He g.s. *if it takes place in reality* should mean non single-particle nature of this state [means not described as $^8\text{He}(\text{g.s.}) + n + n$] and hence a limited applicability of our model.

B. Prospects of correlation studies

Important structure information about the three-body system could be obtained analysing the correlations among the decay products. The recent examples of such data analysis include successful application to the broad states in the continuum of ^5H system [28] and to the two-proton radioactivity decays of ^{19}Mg [29] and ^{45}Fe [30]. Such range of application indicates a potential power of the correlation studies.

The partial decompositions of the cross section given in Fig. 6 show how the contributions of the $[s_{1/2}]^2$ component (mainly $K = 0$) and $[p_{1/2}]^2$ component (mainly $K = 2$) change when we add the s -wave interaction in ^9He channel on top of the p -wave interaction or switch from the narrow to the broad source. The qualitative differences in these decompositions should be seen as qualitative differences in the correlation patterns.

The complete correlation information is provided in Fig. 13 for correlations in the $[s_{1/2}]^2$ state [$E = 4$ keV, panel (a)] and in the $[p_{1/2}]^2$ state at $E = 2.3$ MeV in the calculations with attraction in s -wave (b) and no s -wave attraction (c). The correlation densities are given in the plane of parameters $\{\varepsilon, \cos(\theta_k)\}$ both in “T” and “Y” Jacobi coordinate systems. Parameter $\varepsilon = E_x/E$ describes the energy distribution between X and Y Jacobi subsystems (E_x is energy in the X Jacobi subsystem). Parameter θ_k is angle between Jacobi momenta k_x and k_y in the chosen Jacobi coordinate system:

$$\cos(\theta_k) = \frac{(\mathbf{k}_x, \mathbf{k}_y)}{k_x k_y}.$$

More details can be found in Ref. [31].

The correlation picture for the virtual three-body state with the $[s_{1/2}]^2$ structure is quite featureless [Fig. 13 (a)]. The energy distribution between subsystems is close to the “phase volume” distribution

$$\frac{d^2\sigma}{dE dE_x} \sim E \sqrt{E_x(E - E_x)}. \quad (11)$$

There are only minor deviations from flat distribution for $\cos(\theta_k)$ at $\theta_k \sim 0^\circ$ and $\theta_k \sim 180^\circ$ in “T” Jacobi system (these are configurations when three particles come out in a line).

The predicted correlations for the $[p_{1/2}]^2$ state in “T” Jacobi system [Fig. 13 (c)] look very much like those already observed in other p -wave systems ^6Be [32] and ^5H [28]. There is a double-hump structure reflecting the $[p_{1/2}]^2$ population. The hump, which corresponds to low-energy motion between neutrons is strongly enhanced due to FSI in the n - n channel.

Fig. 13 (b) provides prediction of correlations which is possibly important for prospective ^{10}He studies. If the attractive s -wave interaction is added it qualitatively changes the picture of correlations at the expected $[p_{1/2}]^2$ state position. Now the energy distribution between subsystems (in the “T” Jacobi system) is close to the phase

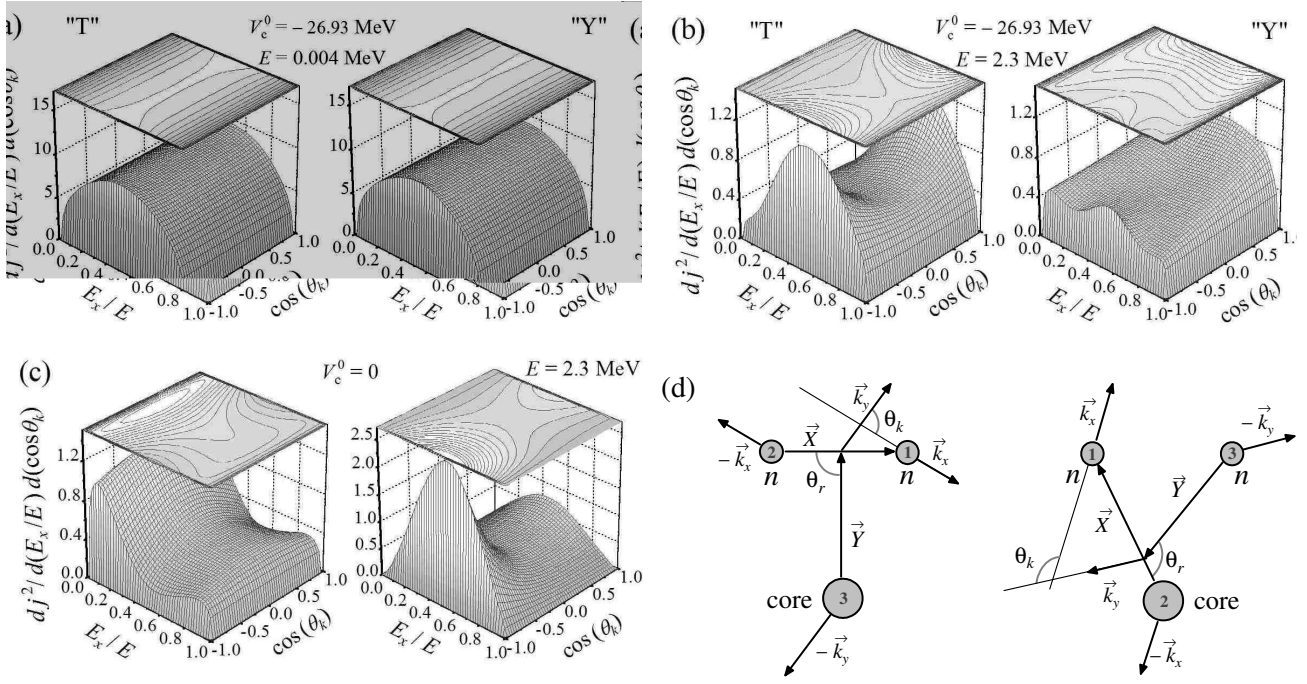


FIG. 13: Complete correlation information about decays of 0^+ state at given energy E . Left and right columns show the same result in “T” and “Y” Jacobi systems. Calculations provided in panels (a), (b), and (c) correspond to the same panels of Fig. 8. Panel (d) shows the coordinates and angles in radial and momentum space for the “T” and “Y” Jacobi systems.

space distribution Eq. (11). Also the angular distribution changes drastically: the correlation density is concentrated in the regions where one of the neutrons is close to the ^8He core in the momentum space [$\cos(\theta_k) \sim \pm 1$ and $E_x/E \sim 5/9$ in the “T” Jacobi system]. In this case the only expressed feature in the “Y” Jacobi system is the “dineutron” correlation which can be seen as a small peak at $\cos(\theta_k) \sim -1$ and $E_x/E \sim 1/2$.

The drastic changes between distributions Fig. 13 (b) and (c) mean that in the experimental measurements giving access to such a characteristic there will be no doubts in the structure identification even in the case of a poor population of the low-energy part of the spectrum or technical problems with detection of the low-energy events.

C. Reliability of the results

It should be mentioned once again that the aspects of the ^{10}He dynamics, discussed in this work, are only valid if the single-particle $^8\text{He}(\text{g.s.})+n+n$ structure of the low-lying ^{10}He states really takes place. The ground for such an assumption is provided by knowledge of the ^9He spectrum. However, the narrow first resonant states of ^9He , as observed in Refs. [3, 4] [$E(p_{1/2}) = 1.27$ MeV, $\Gamma = 0.1$ MeV and $E(p_{3/2}) = 2.4$ MeV, $\Gamma = 0.7$ MeV], presume that it is not true, because small spectroscopic factors are expected [33]. In the case that the results of Ref. [12] are preferable [$E(p_{1/2}) = 2$ MeV, $\Gamma = 2$ MeV],

implying that this is a single-particle state, the basis for our model becomes reliable.

Sensitivity of the predictions to the s -wave interaction in the ^9He channel is very high. The experimental results of Refs. [10] ($a < -10$ fm) and [12] ($a > -20$ fm) are not contradictory, although not too restrictive. Thus, still no solid experimental ground can be found here. We think that this issue is a key point for understanding of the ^{10}He structure.

Important conclusion of these studies is that energy spectrum obtained in experiments with ^{11}Li is strongly affected by the reaction mechanism and we do not reproduce the results of the experiment [6] without taking this effect into account. The question can be raised from theoretical side, how reliable is the statement that for $p_{1/2}$ state in ^9He at about 2 MeV we can not get a state in ^{10}He at 1.2 MeV straightforwardly. In Table II we list paring energy E_p for valence neutrons calculated for ^{10}He in different theoretical approaches. With $p_{1/2}$ state at 2 MeV the paring energy should be about 2.8 MeV, while in various theoretical approaches it is typically around 1 MeV and never exceeds 2 MeV. It is clear that relatively small paring energy in ^{10}He is common for different theoretical models and can be considered as a reliable prediction. Also if we have a look on the nearby isotopes, for $p_{3/2}$ subshell nuclei ^6He and ^8He E_p is 2.6 MeV and 3.04 MeV respectively. For ^{11}Li , where $p_{1/2}$ subshell is populated, paring energy is known to be small: $E_p \sim 0.8$ MeV.

V. CONCLUSION

In conclusion we would like to emphasize the most important results of our studies:

- (i) Within theoretical model for $p_{1/2}$ state in the ${}^9\text{He}$ located at about 2 MeV it is problematic to obtain the ${}^{10}\text{He}$ g.s. at about 1.2 MeV straightforwardly. The required for that paring energy is 2.8 MeV, while for $[p_{1/2}]^2$ configuration it is typically obtained $\sim 1 - 2$ MeV.
- (ii) The attraction in s -wave allows to shift state with $[p_{1/2}]^2$ configuration to significantly lower energy. However, for some extreme values of attraction ($a \leq -5$ fm) lead to formation of low-energy $[s_{1/2}]^2$ state which is seen as a sharp peak in the cross section at energies less than 0.3 MeV. The appearance of such a state is in accord with predictions of Ref. [11].
- (iii) In contrast with approach of Ref. [11], we study the conditions of “coexistence” of $[s_{1/2}]^2$ and $[p_{1/2}]^2$ states in the 0^+ continuum for realistic scenarios. It is shown that the state with $[p_{1/2}]^2$ structure is poorly populated (also suffer significant broadening) in the presence of $[s_{1/2}]^2$ ground state and can be easily lost (small on the s -wave “background”). For that reason the idea of Ref. [11] that the ground $[s_{1/2}]^2$ state of the ${}^{10}\text{He}$ remains unobserved, while the observed so far state is the first excited one with $[p_{1/2}]^2$ structure, does not get support in our studies.

Concerning comparison with experimental data:

- (i) Observation of quite a broad peak in ${}^{10}\text{He}$ at about 1.2 MeV in Ref. [6] could be explained by a specific mechanism of the chosen reaction induced by ${}^{11}\text{Li}$ (namely the huge size of neutron halo in ${}^{11}\text{Li}$). This explanation is possible only in the case of absence of virtual state in ${}^9\text{He}$

channel. For ${}^{10}\text{He}$ ground $[p_{1/2}]^2$ state located at $E \geq 2$ MeV the mentioned reaction mechanism leads to a strong enhancement of the low-energy transition strength even without any significant attraction in s -wave. As a result, the peak in the cross section may be shifted to a lower energy (e.g. ~ 1.2 MeV).

- (ii) The provided theoretical model essentially infer the properties of the ${}^{10}\text{He}$ system basing on the properties of the ${}^9\text{He}$ subsystem. At the moment we can not make the existing data on ${}^9\text{He}$ and ${}^{10}\text{He}$ consistent within this model. Calculations with large negative scattering length (e.g. $a < -5$ fm; experimental limit [10] is $a < -10$ fm) in core- n subsystem necessarily lead to formation of the single narrow peak below 0.3 MeV in the spectrum which should have been seen in the experiment [6].

- (iii) We have to conclude that the existing experimental data do not allow to establish unambiguously the “real” g.s. position for ${}^{10}\text{He}$. Alternative experiments (relative to those utilizing ${}^{11}\text{Li}$ beams) are desirable. Further clarification of controversy between the ${}^9\text{He}$ and ${}^{10}\text{He}$ spectra is indispensable for theoretical understanding of the Helium isobar properties.

VI. ACKNOWLEDGEMENTS

We are grateful to Prof. Yu. Ts. Oganessian for inspiration for this work. We are grateful for careful reading of the manuscript and valuable discussions to Profs. A. A. Korshennikov, G. M. Ter-Akopian, and M. S. Golovkov. LVG is supported by the INTAS Grant 05-1000008-8272, Russian RFBR Grants Nos. 05-02-16404 and 05-02-17535, and Russian Ministry of Industry and Science grant NS-1885.2003.2.

-
- [1] A. I. Baz, V. F. Demin, and M. V. Zhukov, *Sov. J. Nucl. Phys.* **9**, 693 (1969) [*Yad. Fiz.* **9**, 1184 (1969)].
 - [2] J. Stevenson, B. A. Brown, Y. Chen, J. Clayton, E. Kashy, D. Mikolas, J. Nolen, M. Samuel, B. Sherrill, J. S. Winfield, Z. Q. Xie, R. E. Julies, W. A. Richter, *Phys. Rev. C* **37**, 2220 (1988).
 - [3] K. K. Seth, M. Artuso, D. Barlow, S. Iversen, M. Kaletka, H. Nann, B. Parker, R. Soundranayagam, *Phys. Rev. Lett.* **58**, 1930 (1987).
 - [4] H. G. Bohlen, B. Gebauer, D. Kolbert, W. von Oertzen, E. Stiliaris, M. Wilpert, T. Wilpert, *Z. Phys.* **A330**, 227 (1988).
 - [5] A. A. Korshennikov, B. V. Danilin, and M. V. Zhukov, *Nucl. Phys.* **A559**, 208 (1993).
 - [6] A. A. Korshennikov, K. Yoshida, D. V. Aleksandrov, N. Aoi, Y. Doki, N. Inabe, M. Fujimaki, T. Kobayashi, H. Kumagai, C.-B. Moon, E. Yu. Nikolskii, M. M. Obuti, A. A. Ogloblin, A. Ozawa, S. Shimoura, T. Suzuki, I. Tanihata, Y. Watanabe, M. Yanokura, *Phys. Lett.* **B326**, 31 (1994).
 - [7] A. N. Ostrowski, H. G. Bohlen, B. Gebauer, S. M. Grimes, R. Kalpakchieva, Th. Kirchner, T. N. Massey, W. von Oertzen, Th. Stolla, M. Wilpert, Th. Wilpert, *Phys. Lett.* **B338**, 13 (1994).
 - [8] H. G. Bohlen, A. Blazevic, B. Gebauer, W. Von Oertzen, S. Thummerer, R. Kalpakchieva, S. M. Grimes, and T. N. Massey, *Prog. Part. Nucl. Phys.* **42**, 17 (1999).
 - [9] T. Kobayashi, K. Yoshida, A. Ozawa, I. Tanihata, A. Korshennikov, E. Nikolski, and T. Nakamura, *Nucl. Phys.* **A616**, 223c (1997).
 - [10] L. Chen, B. Blank, B. A. Brown, M. Chartier, A. Galonsky, P. G. Hansen, M. Thoennessen, *Phys. Lett.* **B505**, 21 (2001).
 - [11] S. Aoyama, *Phys. Rev. Lett.* **89**, 052501 (2002).
 - [12] M. S. Golovkov, L. V. Grigorenko, A. S. Fomichev, A. V. Gorshkov, V. A. Gorshkov, S. A. Krupko, Yu. Ts. Oganessian, A. M. Rodin, S. I. Sidorchuk, R. S. Slepnev, S. V. Stepantsov, G. M. Ter-Akopian, R. Wolski, A. A. Korshennikov, E. Yu. Nikolskii, V. A. Kuzmin, B. G. Novatskii, D. N. Stepanov, P. Roussel-Chomaz, W. Mittig, *Phys. Rev. C* **76**, 021605(R) (2007).
 - [13] D. Gogny, P. Pires and R. de Tourreil, *Phys. Lett.* **B32**, 591 (1970).
 - [14] L. V. Grigorenko, N. K. Timofeyuk, and M. V. Zhukov, *Eur. Phys. J. A* **19**, 187 (2004).
 - [15] R. J. Ascutto and N. K. Glendenning, *Phys. Rev.* **181**, 1396 (1969).
 - [16] N. B. Shulgina, private communication.

- [17] L. V. Grigorenko, and M. V. Zhukov, Phys. Rev. C **76**, 014008 (2007).
- [18] B. V. Danilin, J. S. Vaagen, T. Rogde, S. N. Ershov, I. J. Thompson, and M. V. Zhukov, Phys. Rev. C **76**, 064612 (2007).
- [19] W. Glöckle, Phys. Rev. C **18**, 564 (1978).
- [20] N. Tanaka, Y. Suzuki, K. Varga, R. G. Lovas, Phys. Rev. C **59**, 1391 (1999).
- [21] A. Delfino, T. Frederico, and L. Tomio, Few-Body Syst. **28**, 259 (2000).
- [22] T. Frederico and M. T. Yamashita, Nucl. Phys. **A790**, 116c (2007).
- [23] L. V. Grigorenko, R. C. Johnson, I. G. Mukha, I. J. Thompson, and M. V. Zhukov, Phys. Rev. C **64**, 054002 (2001).
- [24] M. S. Golovkov, L. V. Grigorenko, A. S. Fomichev, Yu. Ts. Oganessian, Yu. I. Orlov, A. M. Rodin, S. I. Sidorchuk, R. S. Slepnev, S. V. Stepantsov, G. M. Ter-Akopian, R. Wolski, Phys. Lett. **B588**, 163 (2004).
- [25] A. I. Baz, Zh. Eksp. Teor. Fiz. **70**, 397 (1976).
- [26] M. V. Zhukov, B. V. Danilin, D. V. Fedorov, J. M. Bang, I. J. Thompson, and J. S. Vaagen, Phys. Rep. **231**, 151 (1993).
- [27] N. B. Shulgina, B. V. Danilin, L. V. Grigorenko, M. V. Zhukov, and J. M. Bang, Phys. Rev. C **62**, 014312 (2000).
- [28] M. S. Golovkov, L. V. Grigorenko, A. S. Fomichev, S. A. Krupko, Yu. Ts. Oganessian, A. M. Rodin, S. I. Sidorchuk, R. S. Slepnev, S. V. Stepantsov, G. M. Ter-Akopian, R. Wolski, M. G. Itkis, A. S. Denikin, A. A. Bogatchev, N. A. Kondratiev, E. M. Kozulin, A. A. Korshenninnikov, E. Yu. Nikolskii, P. Roussel-Chomaz, W. Mittig, R. Palit, V. Bouchat, V. Kinnard, T. Materna, F. Hanappe, O. Dorvaux, L. Stuttgé, C. Angulo, V. Lapoux, R. Raabe, L. Nalpas, A. A. Yukhimchuk, V. V. Perevozchikov, Yu. I. Vinogradov, S. K. Grishechkin, S. V. Zlatoustovskiy, Phys. Rev. C **72**, 064612 (2005).
- [29] I. Mukha, K. Sümmerner, L. Acosta, M. A. G. Alvarez, E. Casarejos, A. Chatillon, D. Cortina-Gil, J. Espino, A. Fomichev, J. E. Garca-Ramos, H. Geissel, J. Gomez-Camacho, L. Grigorenko, J. Hofmann, O. Kiselev, A. Korshenninnikov, N. Kurz, Yu. Litvinov, I. Martel, C. Nociforo, W. Ott, M. Pfutzner, C. Rodriguez-Tajes, E. Roeckl, M. Stanoiu, H. Weick, and P. J. Woods, Phys. Rev. Lett. **99**, 182501 (2007).
- [30] K. Miernik, W. Dominik, Z. Janas, M. Pfützner, L. Grigorenko, C. R. Bingham, H. Czyrkowski, M. Cwiok, I. G. Darby, R. Dabrowski, T. Ginter, R. Grzywacz, M. Karny, A. Korgul, W. Kusmierz, S. N. Liddick, M. Rajabali, K. Rykaczewski, and A. Stolz, Phys. Rev. Lett. **99**, 192501 (2007).
- [31] L. V. Grigorenko, and M. V. Zhukov, Phys. Rev. C **68**, 054005 (2003).
- [32] O. V. Bochkarev, A. A. Korshenninnikov, E. A. Kuz'min, I. G. Mukha, L. V. Chulkov, G. B. Yan'kov, Nucl. Phys. **A505**, 215 (1989).
- [33] F. C. Barker, Nucl. Phys. **A741**, 42 (2004).
- [34] Y. S. Shen and Z. Ren, Phys. Rev. C **54**, 1158 (1996).
- [35] P. Navratil and B. R. Barrett, Phys. Rev. C **57**, 3119 (1998).
- [36] A. Volya and V. Zelevinsky, Phys. Rev. Lett. **94**, 052501 (2005).
- [37] For example in the inelastic process the virtual state is seen as near threshold peak with non-Lorentzian shape.
- [38] What is called the “Borromean” property of resonances, due to relation to artificially created Borromean states in ACCC method [20], is better characterized as energy condition of a “true three-body decay” or a “democratic decay”. The detailed discussion of three-body decay modes can be found in Ref. [23].
- [39] The attractive potentials with barriers are not necessarily needed to form resonances in the continuum. They can be formed by pure repulsive potentials with broad “shelves”.
- [40] Good example is the structure of the bound and quasi-bound states — isobaric partners. An exception here is the situation of the Thomas-Ehrmann shift, when significant deviations from isobaric symmetry can be observed.

TABLE II: Paring energy (in MeV) for ^{10}He defined as $E_p = S_{2n} - 2S_n$ calculated in different theoretical approaches.

Work	[2]	[5] ^a	[34]	[35]	[11]	[36] ^b	This work ^a
$-S_n$	1.22	0.74	0.84	2.38	1.27	1.60	2.0
$-S_{2n}$	1.18	0.6	1.09	2.78	1.68	1.94	$\sim 2.0 - 2.3$
E_p	1.26	0.88	0.59	1.98	0.86	1.25	$\sim 1.7 - 2.0$

^aWe use $p_{1/2}$ elastic cross section peak energy to define S_n .

^bSee Table 1, column 6 of Ref. [36].